nature nanotechnology

LETTERS

PUBLISHED ONLINE: 22 JANUARY 2012 | DOI: 10.1038/NNANO.2011.251

Transport spectroscopy of symmetry-broken insulating states in bilayer graphene

J. Velasco Jr[1], L. Jing[1], W. Bao[1], Y. Lee[1], P. Kratz[1], V. Aji[1], M. Bockrath[1], C. N. Lau[1]*, C. Varma[1], R. Stillwell[2], D. Smirnov[2], Fan Zhang[3], J. Jung[3] and A. H. MacDonald[3]

Bilayer graphene is an attractive platform for studying new two-dimensional electron physics[1–5], because its flat energy bands are sensitive to out-of-plane electric fields and these bands magnify electron–electron interaction effects. Theory[6–16] predicts a variety of interesting broken symmetry states when the electron density is at the carrier neutrality point, and some of these states are characterized by spontaneous mass gaps, which lead to insulating behaviour. These proposed gaps[6,7,10] are analogous[17,18] to the masses generated by broken symmetries in particle physics, and they give rise to large Berry phase effects[8,19] accompanied by spontaneous quantum Hall effects[7–9,20]. Although recent experiments[21–25] have provided evidence for strong electronic correlations near the charge neutrality point, the presence of gaps remains controversial. Here, we report transport measurements in ultraclean double-gated bilayer graphene and use source–drain bias as a spectroscopic tool to resolve a gap of ~2 meV at the charge neutrality point. The gap can be closed by a perpendicular electric field of strength ~15 mV nm^{-1}, but it increases monotonically with magnetic field, with an apparent particle–hole asymmetry above the gap. These data represent the first spectroscopic mapping of the ground states in bilayer graphene in the presence of both electric and magnetic fields.

The single-particle band structure of bilayer graphene resembles that of a gapless semiconductor, with parabolic valence and conduction bands touching at the highly symmetric K and K' Dirac points. When weak remote hopping processes are included, the momentum space band-touching point splits into four[4], and Liftshitz transitions occur at low carrier densities (for discussion see Supplementary Information). For a perpendicular electric field $E_\perp \neq 0$, a bandgap develops and increases with $E_\perp$, saturating at ~0.3 eV (refs 4,26,27), and the conduction band has a 'Mexican hat' shape. When electron–electron interactions are included, bilayer graphene is expected to be unstable to broken-symmetry states, which can be viewed as layer-pseudospin ferromagnets[6].

Bilayer graphene has been described using a two-band model[8] that is valid near the charge neutrality point with the broken-symmetry state quasiparticle Hamiltonian

$$H = -\left(\frac{p^2}{2m^*}\right)\left[\cos(2\phi_{\mathbf{p}})\sigma_x \pm \sin(2\phi_{\mathbf{p}})\sigma_y\right] - \boldsymbol{\Delta}\cdot\boldsymbol{\sigma} \qquad (1)$$

The first term in equation (1) is the quadratic band Hamiltonian, where $\tan\phi_{\mathbf{p}} = p_y/p_x$, where $\mathbf{p}$ is the angular momentum, m^* is the effective mass of the carriers, $\boldsymbol{\sigma}$ is a Pauli matrix vector that acts on the layer degree of freedom, $\boldsymbol{\Delta}$ represents the order parameter of the broken symmetry state, and the $\pm$ signs refers to the K and K' valleys, respectively. It has been variously predicted[6–10] to be oriented in the $\pm z$-direction, yielding gapped isotropic states with large momentum-space Berry curvature[8], or in the x–y plane, yielding gapless anisotropic (nematic) states[11,12] with vanishing Berry curvatures. A variety of distinct but related massive states occur, depending on the relation of the sign of Δ_z to spin and valley[8]. The attributes of some theoretically proposed bilayer graphene states are summarized in Table 1 and Fig. 1, and the relationship between Δ and quasiparticle electronic properties is discussed in detail in the Supplementary Information.

In the first experimental reports[21,22], which hinted at an ordered state in bilayer graphene, the minimum conductivity $\sigma_{\min}$ was a non-monotonic function of $E_\perp$ with a value ~60 μS at $n = E_\perp = 0$, although the experimental evidence for spontaneous gaps in this work was not conclusive. Recent works using single-gated samples reported either very high $\sigma_{\min} \approx 7e^2/h$ (where e is electron charge and h is Planck's constant), which was attributed to the gapless nematic phase[25], or low $\sigma_{\min} \approx 0.3e^2/h$, which hinted at a gapped state[25]. Thus, the nature of the ground state at the charge neutrality point remains very controversial. Here, we demonstrate that the ground state is indeed insulating and gapful with a magnetic field (B)-dependent gap of the form

$$E_{\text{gap}} = \Delta_0 + \sqrt{a^2B^2 + \Delta_0^2} \qquad (2)$$

where $|\Delta_0| \approx 1$ meV and $a \approx 5.5$ meV T^{-1}. By tracking the dependence of E_{gap} on B and on $E_\perp$, which is believed to induce a transition between a layer-unpolarized and a layer-polarized state, we are able to provide a spectroscopic mapping of bilayer graphene ground states.

Our devices consist of exfoliated bilayer graphene sheets with chromium/gold electrodes suspended between silicon/SiO_2 back gates and metal top gates (Fig. 1a). The devices' field effect mobility $\mu_{\text{FE}} = 1/e(\mathrm{d}\sigma/\mathrm{d}n)$, where σ is the device conductivity, typically calculated by taking the slope of the $\sigma(V_{\text{bg}})$ curves between $n = 0$ and $n \approx 4\times10^{10}$ cm^{-2}, is ~80,000–100,000 cm^2 V^{-1} s^{-1}. By tuning the voltages applied to the back-gate V_{bg} and top-gate V_{tg}, we can independently control $E_\perp$ and the charge density n induced in the bilayer. We find that this capability is of utter importance, as even a small amount of $E_\perp$ or n, which may be inadvertently present in single-gated devices, can obscure the insulating state and significantly elevate $\sigma_{\min}$ (see Supplementary Information).

Figure 1c plots the two-terminal differential conductance $G = \mathrm{d}I/\mathrm{d}V$ at $V = 0$ of the device (colour) versus V_{bg} and B and reveals Landau levels as coloured bands radiating from the charge neutrality point and $B = 0$. Line traces of $G(V_{\text{bg}})$ at constant B exhibit conductance plateaus with values near 0, 1, 2, 3, 4 and

[1]Department of Physics and Astronomy, University of California, Riverside, California 92521, USA, [2]National High Magnetic Field Laboratory, Tallahassee, Florida 32310, USA, [3]Department of Physics, University of Texas at Austin, Austin, Texas 78712, USA. *e-mail: lau@physics.ucr.edu

NATURE NANOTECHNOLOGY DOI: 10.1038/NNANO.2011.251

Table 1 | Attributes of possible ordered states in bilayer graphene at $n = E_\perp = 0$.

	Nematic order	QAH	QSH	LAF	CLP (QVH)
Gapped?	No	Yes	Yes	Yes	Yes
Two-terminal σ_{min}	Finite	$4e^2/h$	$4e^2/h$	0	0
Broken symmetries	In-plane rotation	Time reversal; Ising valley	Spin rotational; Ising valley	Time reversal; spin rotation	Inversion

QAH, quantum anomalous Hall; QSH, quantum spin Hall; LAF, layer antiferromagnet; CLP, charge layer polarized; QVH, quantum valley Hall.

$8e^2/h$ (Fig. 1d), indicating that the eightfold degeneracy of the lowest Landau level (LL)[28–31] is broken. Observation of these plateaux at relatively low B underscores the high quality of the device.

Close inspection of Fig. 1d reveals that the $\nu = 0$ gap appears to persist down to $B = 0$. Indeed, at $B = 0$, the $G(E_\perp, n)$ plot shows a local minimum at $n = E_\perp = 0$ (Fig. 2a,b). This contradicts the single-particle picture, which predicts a gap that is roughly linear in $E_\perp$, hence a monotonically decreasing $G(|E_\perp|)$. Our data therefore suggest a breakdown of the non-interacting electron picture, even allowing for the possibility of uncontrolled mechanical deformations in our suspended flakes (Supplementary Information)[32].

To investigate the resistive state at the charge neutrality point spectroscopically, we measure G as a function of source–drain bias V and $E_\perp$ while keeping $n = 0$. Typical spectroscopic transport measurements are performed using tunnel probes, but our devices have highly transparent contacts. Because they are in the quasi-ballistic limit, we nevertheless anticipate spectroscopic resolution. Our nonlinear transport data are summarized in Fig. 2c–f. The most striking feature is the region of dark blue/purple at the centre of the plots, corresponding to the highly resistive state at small $E_\perp$. At $n = E_\perp = V = 0$, the device is insulating, with $G_{min} < \sim 0.5\ \mu S$ (Fig. 2f, green curve). We note that this insulating state is observed only in high-mobility samples realized after current annealing, and then only at low sweeping rates (Supplementary Information) and after careful optimization of the measurement set-up to eliminate spurious voltage noise. As V increases, G remains approximately 0 until it increases abruptly at $V \approx \pm 1.9$ mV, reaching sharp peaks before it decreases again to $\sim 300\ \mu S$. The $G(V)$ curve bears a striking resemblance to the tunnelling density of states of a gapped insulator, and strongly suggests the formation of an ordered phase with an energy gap $E_{gap} \approx 1.9$ meV. This value is further corroborated by temperature-dependent measurements of σ_{min} for a sample in the gapped regime, and by the n-dependence of the gap (Supplementary Information). Importantly, this gap can be closed by application of $E_\perp$ of either polarity: G increases with $|E_\perp|$ (Fig. 2d), and upon application of moderate $E_\perp > \sim 15\ \mathrm{mV\ nm^{-1}}$, the gap-like structure completely vanishes and the $G(V)$ curve becomes approximately V-shaped, with a finite conductance minimum of $\sim 100\ \mu S$ at $n = 0$ (Fig. 2f, purple curve). Finally, for sufficiently large $E_\perp$, $G(V = 0)$ begins to decrease with increasing $E_\perp$ (Fig. 2d), reverting to single-particle behaviour.

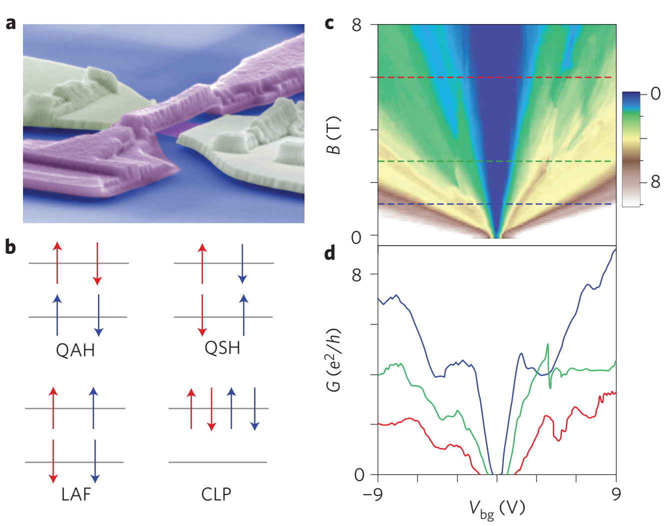

Figure 1 | Device image, proposed gapped states in bilayer graphene and quantum Hall data at 300 mK. a, False-coloured scanning electron microscopy (SEM) image of a device with suspended bilayer graphene (pink), clamped by source–drain electrodes (gold) and straddled from above by a suspended top gate (lavender). The bottom gate (blue) lies beneath the suspended bilayer graphene. The electrode separation is 1.3 µm. **b**, Spin-valley configurations of the electrons in bilayer graphene for several possible phases. Red (blue) arrows indicate electrons from the K (K') valley. **c**, Differential conductance $G = dI/dV$ in units of e^2/h versus B and V_{bg} showing the Landau fan diagram. The colour scale represents conductance. **d**, Line traces $G(V_{bg})$ along the dotted lines in **c** at $B = 1.3$ (blue), 2.8 (green) and 6 T (red), respectively.

Such an insulating state, which is the most salient experimental feature, is only observed in devices with the highest mobility. To gain further insight, we studied its evolution with B (Fig. 3). When B increases from 0, the gapped phase continuously evolves into a bilayer insulating state at filling factor $\nu = 0$, with the sharp peaks in G becoming sharper and more dramatic. The magnitude of the gap, as measured from the bias values of the sharp peaks in G, is well-described by equation (2), where $|\Delta_0| \approx 1$ meV (obtained from Fig. 2f) and $a = 5.5\ \mathrm{mV\ T^{-1}}$. For $B > 0.5$ T, $E_{gap} \approx 5.5B$ (meV $\mathrm{T^{-1}}$), which is much larger than the single-particle gap induced by Zeeman splitting, $\sim 0.1\ \mathrm{meV\ T^{-1}}$. We note that our observation of a linear dependence of $\Delta_{\nu=0}$ on B is consistent with previous reports[7,30], but with a significantly larger magnitude, possibly owing to the superior quality of our device. Another noteworthy feature of Fig. 3a is that the conductance peaks at positive and negative bias voltages, which we associate with conduction and valence band edges, are highly asymmetric. Because the current–voltage characteristics of the device are symmetric in V outside the gapped region, this observed asymmetry, which increases with increasing B and reverses when B changes sign, does not arise from contact asymmetry, nor can it be accounted for by the Onsager relation because the measurements are carried out in the nonlinear regime. Rather, it suggests particle–hole asymmetry in the device.

Our experimental findings may be summarized as follows: (i) ultraclean bilayer graphene is insulating at $n = B = E_\perp = 0$, with an energy gap $E_{gap} \approx 1.9$ meV that can be closed by $E_\perp$ of either sign; (ii) the energy gap evolves in B following equation (2); and (iii) this state is apparently particle–hole asymmetric. These observations provide much insight into the nature of bilayer graphene's symmetry-broken ground state. For instance, observation (i) rules out gapless ordered states[11,12]. For the gapped states, the symmetric dependence on $E_\perp$ indicates that there is no net charge imbalance between the two layers, thus excluding states with net spontaneous layer polarization like the charge layer polarized (CLP) state depicted in Fig. 1. We note that the CLP phase, also called the quantum valley Hall (QVH) state, is expected to be the ground state under sufficiently large $E_\perp$, as observed experimentally.

Thus, among the proposed states, we are left with the three gapped state candidates that have no overall layer polarization. Given the

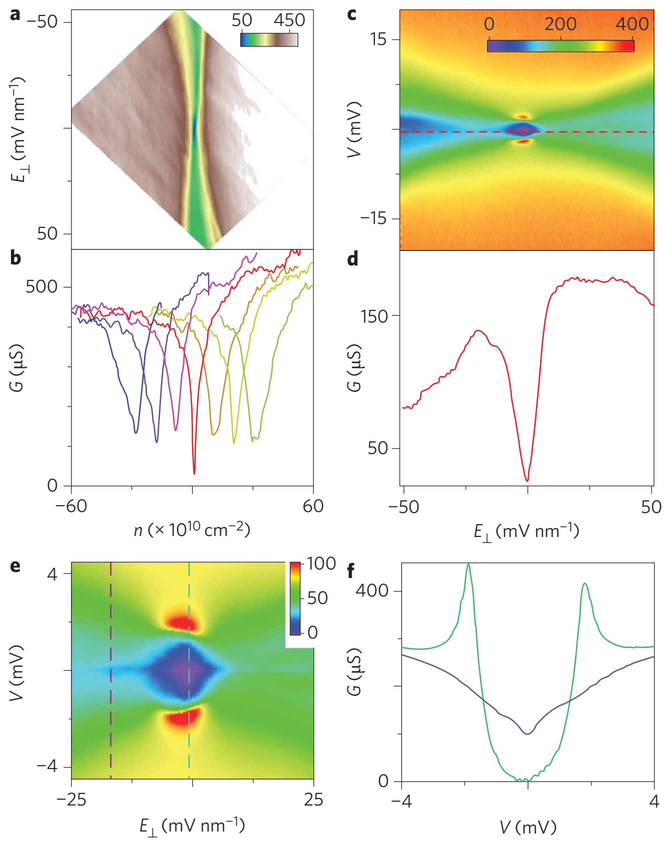

Figure 2 | Transport data at $B = 0$ and $T = 300$ mK. a,**b**, $G(n, E_\perp)$ and line traces $G(n)$ at $E_\perp = -37.5$, -25, -12.5, 0, 12.5, 25 and 37.5 mV nm^{-1}, respectively (left to right). The line traces are laterally offset for clarity and the colour scale is in units of conductance, μS. **c**,**d**, Large-range $G(V, E_\perp)$ in units of μS and line trace $G(E_\perp)$ at $n = 0$. **e**, High-resolution $G(V, E_\perp)$ for small bias range at $n = 0$. **f**, Line traces $G(V)$ along the dotted lines in **e** at $E_\perp = 0$ (purple) and -15 mV nm^{-1} (green), respectively.

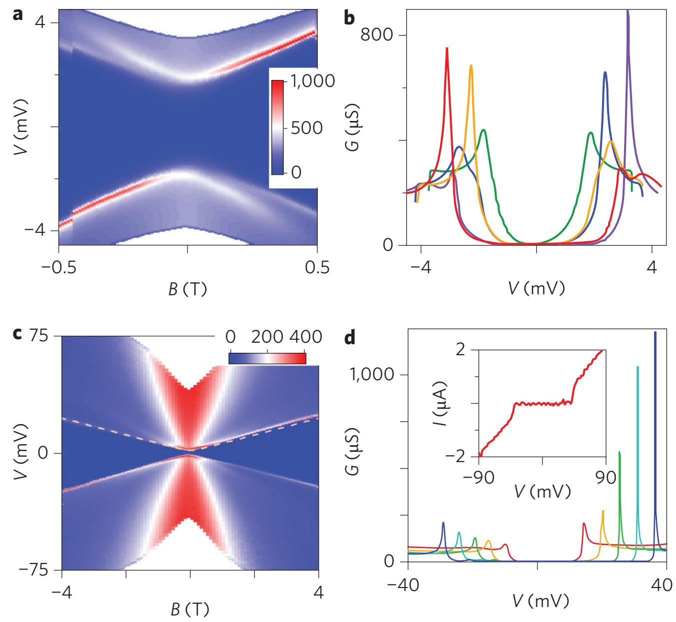

Figure 3 | Transport data in magnetic field at $n = 0$ and $E_\perp = 0$. **a**,**b**, $G(V, B)$ (in units of μS) and line traces $G(V)$ at $B = -0.4$ (red), -0.2 (orange), 0 (green), 0.2 (blue) and 0.4 T (purple), respectively. **c**, Large-range $G(V, B)$. The dotted line plots equation (2) with $\Delta_0 = 1$ meV, and $a = 5.5$ meV T^{-1}. The colour scale is in units of conductance, μS. **d**, Line traces $G(V)$ at $B = 2$ (red), 3 (orange), 4 (green), 5 (cyan) and 6 T (blue). Inset: current–voltage characteristics at $B = 8$ T.

flavour (spin-valley) symmetries, electrons in each layer can be valley-polarized and form a quantum anomalous Hall (QAH) insulator[7,8,33,34], spin-polarized to form a layer antiferromagnet (LAF)[8,20] or neither to form a quantum spin Hall (QSH) insulator[7,8,35–37] (Fig. 1b). Mean-field calculations indicate that these states are comparable[9] in energy and that the CLP state is stabilized by electric fields $E_\perp \approx 5$–20 mV nm^{-1} (refs 7,9), in agreement with the critical field value of ~15 mV nm^{-1} observed experimentally. For all three states, equation (1) predicts a gap within each valley with a B-dependence described by equation (2), with parameters $\Delta_z = \Delta_0$ and $a = \sqrt{2}\hbar e/m^*$. From $a = 5.5$ meV T^{-1}, we obtain $m^* = 0.03m_e$, where m_e is electron rest mass, in good agreement with other measurements[38] of the interaction enhanced[39,40] quasiparticle mass near the bilayer graphene charge neutrality point. Our observations therefore demonstrate unequivocally the symmetry-broken gapped phase in charge neutral graphene.

Nailing down the exact phase of the ground state, however, is considerably more difficult. Equation (2) applies to charges in a single valley. If we assume ideal coupling of both layers to the electrodes, none of the candidate states can account for all aspects of our data. The LAF state would have a B-independent gap. Both QAH and QSH states are ruled out by their topologically protected edge states, which are expected to yield two-terminal conductances ~$4e^2/h$ or 154 μS. The QAH state is also ruled out because the density position of its gap is expected to deviate from the charge neutrality point in a finite magnetic field, following lines with $\nu = 4$, yet it is the only state with particle–hole asymmetry and valley-indirect gaps that are in agreement with equation (2).

On the other hand, we note that because most of the metals are deposited on the top layer and contact the bottom layer only via the edges, the electrodes could couple preferentially to one layer (or equivalently, one valley). In this case, the LAF state, which is the only proposed insulating phase, can account for both observations (i) and (ii). Because the absence of edge states is the most robust experimental signature, our observations are most consistent with the LAF state, although the particle–hole asymmetry in B is not explained within this picture. It is thus possible that a new ground state that has not been theoretically proposed underlies our observations. Further theoretical and experimental work will be necessary to ascertain the nature of the gapped state and achieve a full understanding of our observations.

Finally, we focus on the quantum Hall states in external electric and magnetic fields and further establish the bias-dependent measurement as a spectroscopic tool. Figure 4a plots G versus $E_\perp$ and n at constant $B = 3.5$ T. As shown by the line traces in Fig. 4b,c, at $E_\perp = 0$, only the $\nu = 0$ and $\nu = 4$ quantum Hall plateaux are observed; at finite $E_\perp$, all integer quantum Hall states between 0 and 4 are resolved, demonstrating degeneracy-lifting by the perpendicular electric field. From the spectroscopic data $G(V, E_\perp)$ at constant B, the gap $\Delta_{\nu=0}$ is diamond-shaped (Fig. 4d,e): its magnitude decreases linearly with applied $E_\perp$ of either polarity, until it is completely closed at a critical field $E_\perp^*$. Figure 4f plots $E_\perp^*$ obtained at three different B values. The data points fall on a straight line, with a best-fit slope of ~12.7 mV nm^{-1} T^{-1}. Extrapolation of the best-fit line to $B = 0$ yields a finite $E_\perp^*$ intercept ~12.5 mV nm^{-1}, which agrees with the critical $E_\perp$ value estimated from the zero B field data in Fig. 2d. Both the slope and the finite $E_\perp^*$ intercept are consistent with those measured from the movement of the $\nu = 4$ plateau as functions of $E_\perp$ and B (ref. 22; see Supplementary Information). Taken together, our data confirm that the bias-dependent measurement provides a spectroscopic

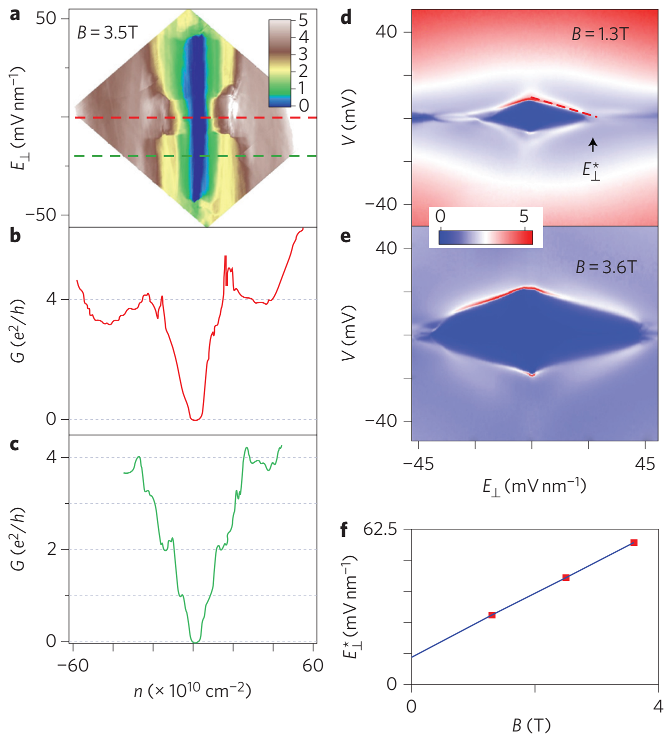

Figure 4 | Transport data at constant *B*. a, $G(n, E)$ in units of e^2/h at $B = 3.5$ T. **b**,**c**, Line traces $G(n)$ along the dotted lines in **a** at $E_\perp = 0$ (red) and -20 mV nm^{-1} (green). **d**,**e**, $G(V, E)$ at $B = 1.3$ T and 3.6 T, respectively. Both colour scales are in conductance units of e^2/h. **f**, Critical electric field $E_\perp{}^*$ versus B. The blue line is a best fit to data, with a slope of 12.7 mV nm^{-1} T^{-1}.

determination of the $\nu = 0$ gap, and indicates a transition between two different quantum Hall ferromagnetic phases[15]. Interestingly, a recent theoretical analysis[15] suggests the nature of these two phases is a canted antiferromagnetic and a CLP state. Such a finding is consistent with our previous conclusion of the LAF phase at $B = E_\perp = n = 0$.

In summary, we demonstrate the formation of a gapped, insulating phase in charge-neutral bilayer graphene. The gap is closed by application of a perpendicular E field of either polarity and evolves into a $\nu = 0$ state in a magnetic field with a gap of $\sim$5.5 meV T^{-1}, with apparent particle–hole symmetry. Our work, together with recent experiments[21–25], contributes towards understanding the rich interaction-driven physics in bilayer graphene. Further theoretical and experimental work, such as scanning tunnelling microscopy or optical Kerr effect measurements, is warranted to ascertain the nature of the gapped states.

Received 19 October 2011; accepted 19 December 2011; published online 22 January 2012

References

1. Zhang, Y. B., Tan, Y. W., Stormer, H. L. & Kim, P. Experimental observation of the quantum Hall effect and Berry's phase in graphene. *Nature* **438,** 201–204 (2005).
2. Novoselov, K. S. *et al.* Two-dimensional gas of massless Dirac fermions in graphene. *Nature* **438,** 197–200 (2005).
3. Novoselov, K. S. *et al.* Electric field effect in atomically thin carbon films. *Science* **306,** 666–669 (2004).
4. McCann, E. & Fal'ko, V. I. Landau-level degeneracy and quantum Hall effect in a graphite bilayer. *Phys. Rev. Lett.* **96,** 086805 (2006).
5. Castro Neto, A. H., Guinea, F., Peres, N. M. R., Novoselov, K. S. & Geim, A. K. The electronic properties of graphene. *Rev. Mod. Phys.* **81,** 109–162 (2009).
6. Min, H., Borghi, G., Polini, M. & MacDonald, A. H. Pseudospin magnetism in graphene. *Phys. Rev. B* **77,** 041407 (2008).
7. Nandkishore, R. & Levitov, L. Quantum anomalous Hall state in bilayer graphene. *Phys. Rev. B* **82,** 115124 (2010).
8. Zhang, F., Jung, J., Fiete, G. A., Niu, Q. A. & MacDonald, A. H. Spontaneous quantum Hall states in chirally stacked few-layer graphene systems. *Phys. Rev. Lett.* **106,** 156801 (2011).
9. Jung, J., Zhang, F. & MacDonald, A. H. Lattice theory of pseudospin ferromagnetism in bilayer graphene: competing interaction-induced quantum Hall states. *Phys. Rev. B* **83,** 115408 (2011).
10. Zhang, F., Min, H., Polini, M. & MacDonald, A. H. Spontaneous inversion symmetry breaking in graphene bilayers. *Phys. Rev. B* **81,** 041402 (R) (2010).
11. Lemonik, Y., Aleiner, I. L., Toke, C. & Fal'ko, V. I. Spontaneous symmetry breaking and Lifshitz transition in bilayer graphene. *Phys. Rev. B* **82,** 201408 (2010).
12. Vafek, O. & Yang, K. Many-body instability of Coulomb interacting bilayer graphene: renormalization group approach. *Phys. Rev. B* **81,** 041401 (2010).
13. Castro, E. V., Peres, N. M. R., Stauber, T. & Silva, N. A. P. Low-density ferromagnetism in biased bilayer graphene. *Phys. Rev. Lett.* **100,** 186803 (2008).
14. Martin, I., Blanter, Y. M. & Morpurgo, A. F. Topological confinement in bilayer graphene. *Phys. Rev. Lett.* **100,** 036804 (2008).
15. Kharitonov, M. Canted antiferromagnetic phase of the $\nu = 0$ quantum Hall state in bilayer graphene. Preprint at arXiv:1105.5386v1101 (2011).
16. Zhang, F. & MacDonald, A. H. Distinguishing spontaneous quantum Hall states in graphene bilayers. Preprint at arXiv:1107.4727v1101 (2011).
17. Gorbar, E. V., Gusynin, V. P. & Miransky, V. A. Dynamics and phase diagram of the $\nu = 0$ quantum Hall state in bilayer graphene. *Phys. Rev. B* **81,** 155451 (2010).
18. Herbut, I. F., Juricic, V. & Vafek, O. Relativistic Mott criticality in graphene. *Phys. Rev. B* **80,** 075432 (2009).
19. Xiao, D., Chang, M. C. & Niu, Q. Berry phase effects on electronic properties. *Rev. Mod. Phys.* **82,** 1959–2007 (2010).
20. Vafek, O. Interacting fermions on the honeycomb bilayer: from weak to strong coupling. *Phys. Rev. B* **82,** 205106 (2010).
21. Martin, J., Feldman, B. E., Weitz, R. T., Allen, M. T. & Yacoby, A. Local compressibility measurements of correlated states in suspended bilayer graphene. *Phys. Rev. Lett.* **105,** 256806 (2010).
22. Weitz, R. T., Allen, M. T., Feldman, B. E., Martin, J. & Yacoby, A. Broken-symmetry states in doubly gated suspended bilayer graphene. *Science* **330,** 812–816 (2010).
23. Bao, W. *et al.* Stacking-dependent band gap and quantum transport in trilayer graphene. *Nature Phys.* **7,** 948–952 (2011).
24. Freitag, F., Trbovic, J., Weiss, M. & Schonenberger, C. Spontaneously gapped ground state in suspended bilayer graphene. Preprint at arXiv:1104.3816vs (2011).
25. Mayorov, A. S. *et al.* Interaction-driven spectrum reconstruction in bilayer graphene. *Science* **333,** 860–863 (2011).
26. Min, H. K., Sahu, B., Banerjee, S. K. & MacDonald, A. H. *Ab initio* theory of gate induced gaps in graphene bilayers. *Phys. Rev. B* **75,** 155115 (2007).
27. Ohta, T., Bostwick, A., Seyller, T., Horn, K. & Rotenberg, E. Controlling the electronic structure of bilayer graphene. *Science* **313,** 951–954 (2006).
28. Barlas, Y., Cote, R., Nomura, K. & MacDonald, A. H. Intra-Landau-level cyclotron resonance in bilayer graphene. *Phys. Rev. Lett.* **101,** 097601 (2008).
29. Zhao, Y., Cadden-Zimansky, P., Jiang, Z. & Kim, P. Symmetry breaking in the zero-energy Landau level in bilayer graphene. *Phys. Rev. Lett.* **104,** 066801 (2010).
30. Feldman, B. E., Martin, J. & Yacoby, A. Broken-symmetry states and divergent resistance in suspended bilayer graphene. *Phys. Status Solidi B* **5,** 889–893 (2009).
31. Bao, W. *et al.* Magnetoconductance oscillations and evidence for fractional quantum Hall states in suspended bilayer and trilayer graphene. *Phys. Rev. Lett.* **105,** 246601 (2010).
32. Mucha-Kruczynski, M., Aleiner, I. L. & Fal'ko, V. I. Strained bilayer graphene: band structure topology and Landau level spectrum. *Phys. Rev. B* **84,** 041404(R) (2011).
33. Haldane, F. D. M. Model for a quantum Hall-effect without landau-levels—condensed-matter realization of the parity anomaly. *Phys. Rev. Lett.* **61,** 2015–2018 (1988).
34. Nagaosa, N., Sinova, J., Onoda, S., MacDonald, A. H. & Ong, N. P. Anomalous Hall effect. *Rev. Mod. Phys.* **82,** 1539–1592 (2010).
35. Kane, C. L. & Mele, E. J. Quantum spin Hall effect in graphene. *Phys. Rev. Lett.* **95,** 226801 (2005).
36. Konig, M. *et al.* Quantum spin Hall insulator state in HgTe quantum wells. *Science* **318,** 766–770 (2007).
37. Raghu, S., Qi, X. L., Honerkamp, C. & Zhang, S. C. Topological Mott insulators. *Phys. Rev. Lett.* **100,** 156401 (2008).
38. Henriksen, E. A. *et al.* Cyclotron resonance in bilayer graphene. *Phys. Rev. Lett.* **100,** 087403 (2008).
39. Castro, E. V., Peres, N. M. R. & dos Santos, J. M. B. L. Gaped graphene bilayer: disorder and magnetic field effects. *Phys. Stat. Sol. B* **244,** 2311–2316 (2007).

40. Borghi, G., Polini, M., Asgari, R. & MacDonald, A. H. Fermi velocity enhancement in monolayer and bilayer graphene. *Solid State Commun.* **149,** 1117–1122 (2009).

Acknowledgements

The authors thank R. Nandkishore, B. Feldman, A. Yacoby, L. Levitov, P. Jarillo-Herrero and K. Novoselov for stimulating discussions, and D. Humphrey, G. Liu, A. Zhao and H. Zhang for assistance with fabrication. This work was supported in part by the UC LabFees programme, NSF CAREER DMR/0748910, NSF/1106358, ONR N00014-09-1-0724, ONR/DMEA H94003-10-2-1003 and the FENA Focus Center. D.S. acknowledges support from NHMFL UCGP #5068. Part of this work was performed at NHMFL, which is supported by NSF/DMR-0654118, the State of Florida, and DOE. A.M., J. J. and F.Z. acknowledge support from the Welch Foundation (grant TBF1473), NRI-SWAN and DOE (grant DE-FG03-02ER45958). C.V. acknowledges support from NSF DMR-0906530. V.A. acknowledges support from UCR I.C.

Author contributions

C.N.L and J.V. conceived the experiments. Y.J. and P.K. isolated and identified the graphene sheets. R.S. assisted with sample preparation. J.V., L.J., W.B., Y.J. and D.S. performed transport measurements. C.N.L, M.B., W.B. and J.V. interpreted and analysed the data. V.A., C.V., F.Z., J.J. and A.H.M. interpreted data and performed theoretical calculations. C.N.L., J.V., F.Z., J.J. and A.H.M. co-wrote the paper. All authors discussed the results and commented on the manuscript.

Additional information

The authors declare no competing financial interests. Supplementary information accompanies this paper at www.nature.com/naturenanotechnology. Reprints and permission information is available online at http://www.nature.com/reprints. Correspondence and requests for materials should be addressed to C.N.L.